

Effects in 94 GHz Orientation-Selected PELDOR on a Rigid Pair of Radicals with Non-Collinear Axes

G. Sicoli · T. Argirević · J. Stubbe · I. Tkach ·
Marina Bennati

Received: 18 May 2009 / Revised: 19 June 2009 / Published online: 13 November 2009
© The Author(s) 2009. This article is published with open access at Springerlink.com

Abstract For aromatic organic radicals, pulsed electron-electron double resonance (PELDOR) experiments at high magnetic fields provide information not only about the distance between the paramagnetic species but also about their relative orientation. However, the three-dimensional biradical structure is encoded in a complex pattern of orientation-selected PELDOR traces and the execution of the experiment is generally aggravated by constraints posed by the available hardware and the intrinsically low modulation depth observed. We present a 94 GHz PELDOR experiment performed with a commercial spectrometer and probe heads that permit separation of pump and detection frequencies up to 150 MHz. The setup is employed to examine the orientation selections on a general case of rigid biradicals with non-collinear g axes. The interacting radicals, a tyrosyl radical ($Y_{122}\cdot$) located in the $\beta 2$ subunit and an 3-aminotyrosyl radical ($NH_2Y_{731}\cdot$) located in the $\alpha 2$ subunit, are generated by *Escherichia coli* ribonucleotide reductase with a 3-aminotyrosine (NH_2Y) site specifically incorporated into $\alpha 2$ in the presence of cytidine 5'-diphosphate and adenosine 5'-triphosphate. The experimental designs as well as some characteristic features of the observed modulation pattern are discussed.

G. Sicoli (✉) · T. Argirević · I. Tkach · M. Bennati (✉)
Max Planck Institute for Biophysical Chemistry, Göttingen, Germany
e-mail: gsicoli@gwdg.de

M. Bennati
e-mail: bennati@mpibpc.mpg.de

J. Stubbe
Departments of Chemistry and Biology, Massachusetts Institute of Technology,
Cambridge, MA, USA

1 Introduction

Pulsed electron-electron double resonance (PELDOR or DEER) spectroscopy has been established over the past few years as a valuable method to obtain distances and their distributions between paramagnetic centers in biological systems [1–5]. The majority of the experiments have been performed at X-band frequencies, where the electron paramagnetic resonance (EPR) spectra of radicals are mostly dominated by hyperfine couplings and their spectral widths in frozen solutions do not usually exceed 100 G. For instance, the spectrum of a nitroxide spin label has a width of about 75 G and that of a tyrosyl radical ($Y\cdot$) about 45 G. With the microwave power available in commercial X-band spectrometers, strongly overcoupled resonators are used to pump and detect at arbitrary positions of the EPR line, and pump pulses as short as 12 ns are routinely employed to cover the largest possible portion of the EPR spectrum to maximize the modulation depth.

At high EPR frequencies ($\nu \geq 90$ GHz) the situation is quite different. The EPR line becomes dominated by the anisotropy of the g -tensor, which scales linearly with the external field. At 94 GHz the EPR spectra of nitroxide and tyrosyl radicals display similar spectral widths ($B \parallel g_x$ to $B \parallel g_z$) of about 125–150 G. On the other hand, current state-of-the-art instrumentation for W-band allows typical microwave π pulses as short as 24 ns, when using impact ionization avalanche transit-time (IMPATT) amplifiers in combination with high- Q cavities [6], or even shorter if using special 1 kW microwave sources [7, 8]. When using commercial W-band spectrometers that rely on IMPATT technology, it has to be considered that pulse lengths of 24 ns excite only a small fraction of the high-field EPR line and orientational selectivity becomes an intrinsic property of the PELDOR response.

Recently, orientational selectivity in high-frequency PELDOR has been reported and analyzed in detail for three different cases [9–12]: (1) for rigid amino acid biradicals in proteins, (2) for synthetic nitroxide bi- and triradicals undergoing restricted dynamics [10], and (3) for a light-induced spin-correlated radical pair [11]. In all three cases the observed modulation traces resulted as a complex function of the pump and detection position in the EPR line, and extensive analysis was required to interpret the data. In the first case we showed that, because of the excellent signal-to-noise (S/N) ratio, from the 180 GHz PELDOR data [12, 13] and the independent knowledge of magnetic parameters (g -tensors, hyperfine couplings and inter-radical distance) we were able to reconstruct a biradical structure (i.e., to determine the relative orientation of the two g -tensors with respect to their interconnecting dipolar axis).

One general requirement of the PELDOR experiment is that the dipolar modulation can be detected only if the pump and observer pulses, respectively, excite each radical belonging to the interacting pair. In contrast with the studies reported at X-band with nitroxide radicals [14, 15], where the pump pulse excites all orientations and only the probe pulse is selective, at high frequencies both pulses are selective and little or no response will be observed for many combinations of pump and detection frequencies [9]. In the latter case, for a detailed examination of possible orientations and to obtain sufficient constraints in the analysis, the separation between pump and detection frequencies as well as the detection position

in the EPR line needs to be systematically varied. However, the available hardware for high-frequency EPR spectroscopy still poses some severe limitations in the experimental procedure. Specifically, the separation of pump and detection frequencies is limited by the high quality factor Q of the resonator. In the experiments reported so far either the frequency separation was kept constant by varying the external field [9, 10] or a field jump technique was implemented [11].

In this paper, we explore the capability of performing orientation-selected 94 GHz PELDOR on a rigid pair of amino acid radicals with non-collinear g axes. Using new commercial hardware, we record PELDOR traces by varying both the resonant field position at detection as well as the separation between pump and detection frequencies.

The radicals are trapped during the incubation of substrate (cytidine 5'-diphosphate, CDP) and allosteric effector (adenosine 5'-triphosphate, ATP) with *Escherichia coli* ribonucleotide reductase (RNR), in which an unnatural amino acid 3-NH₂Y has been site specifically incorporated in place of Y₇₃₁ in the α subunit. One radical, a tyrosyl (Y₁₂₂[•]), is located in the β 2 subunit and a 3-aminotyrosyl radical (NH₂Y₇₃₁[•]) is located in the α 2 subunit. The active RNR complex is a α 2 β 2 pair and one of the radicals is located in one $\alpha\beta$ pair, while the other is located in the second $\alpha\beta$ pair. Our previous X-band data indicated that the inter-radical distance is 3.8 nm [16]. The high-field EPR spectrum of a 3-NH₂Y[•] has been recently characterized in detail at 180 and 94 GHz [17]. The availability of a docking model [18] for the α 2 β 2 complex is used to rationalize the observed modulation effects.

2 Experimental

The experiments were performed on a commercial Bruker pulse W-band spectrometer Eleksys 680 equipped with a Power Upgrade 2 that delivers 400 mW power from the microwave bridge and amplifier. For the PELDOR experiments, we employed two Bruker W-band resonators of the series E600-1021H. The standard high- Q resonator has a bandwidth of 20 MHz, whereas a second one was specially tuned to low- Q with a bandwidth of about 150 MHz. The behavior of the B_1 microwave field through the low- Q resonant mode was measured with transient nutation experiments at $T = 10$ K. At the minimum of the cavity dip the π pulse was 40 ns as compared to 24 ns with the high- Q setup.

All experiments were performed using the four-pulse DEER sequence [2] and setting the observer frequency in the center of the cavity dip, which accounts for maximal sensitivity at detection. The values of the pump pulse were adjusted for each position of the pump frequency with respect to the cavity dip according to Fig. 2a. The dipolar evolution time T (spacing between the first and the second π pulses in the detection sequence) was selected to be 2.5 μ s based on the modulation frequency $\nu_{\perp} = 0.8$ MHz observed at X-band [16]. However, last 0.5 μ s of the time traces had to be cut due to a spectrometer artifact that distorts the baseline. The number of scans acquired varied between 100 and 200 (with 10 shots/pt), depending on the detection position in the EPR line. Due to the low temperature ($T \approx 10$ K) required to detect the Y₁₂₂[•] in RNR, shot repetition times up to 75 ms were used and

acquisition times at each field value lasted up to 5 h. To avoid shifts of the microwave mode during the long accumulation time, cryostat and probe head were thermally equilibrated for 2–3 h.

The radical pair was generated by mixing a 80–100 μM solution of the *E. coli* RNR- $\text{Y}_{731}\text{NH}_2\text{Y}\text{-}\alpha 2$, with $\beta 2$ containing 1.1 Y \cdot s, and with CDP and ATP. The reaction was stopped after 30 s, placed in the W-band tube with an outer diameter of 0.9 mm, and the sample was frozen in liquid nitrogen. The yield of the radical pair ($\text{NH}_2\text{Y}_{731}\cdot$ and $\text{Y}_{122}\cdot$) was previously estimated to be about 25% of the initial $\text{Y}_{122}\cdot$ concentration [16].

3 Results and Discussion

The 94 GHz pulsed echo-detected spectrum of the two radicals at $T = 10$ K is displayed in Fig. 1. The line shape can be decomposed into the contribution of the single species by recording the spectrum of $\text{NH}_2\text{Y}_{731}\cdot$ at 70 K (Fig. 1, dotted line). At this temperature, the relaxation of $\text{Y}_{122}\cdot$ is sufficiently fast that this radical can be filtered out in a spin echo experiment. A separate measurement (before addition of CDP and ATP) gives the spectrum of $\text{Y}_{122}\cdot$ as a reference (Fig. 1, dashed line). The g values are marked, respectively. The g_x shift of $\text{Y}_{122}\cdot$ (2.0092) is substantially larger than in $\text{NH}_2\text{Y}_{731}\cdot$ (2.0052), consequently the low-field side of the 94 GHz spectrum contains exclusively contribution of $\text{Y}_{122}\cdot$. On the other hand, the g_y and g_z values of the two radicals are very similar ($g_y = 2.0046$, $g_z = 2.0025$) and the two species cannot be distinguished in this spectral region.

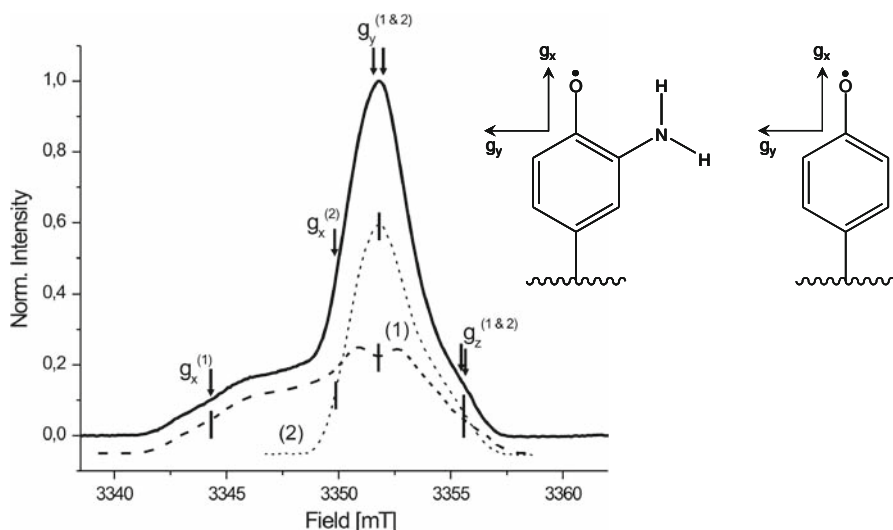


Fig. 1 94 GHz spin-echo-detected spectrum of the reaction mixture (*solid line*) at $T = 10$ K. The *dashed line* represents the reference spectrum of $\text{Y}_{122}\cdot$ (marked with the index 1), the *dotted line* the spectrum of $\text{NH}_2\text{Y}_{731}\cdot$ (marked with the index 2). The g values of the radicals are marked. In the *inset* the chemical structures of the two radicals are depicted. The orientation of the g_x axis in $\text{NH}_2\text{Y}_{731}\cdot$ has been determined in Ref. [17]

In Fig. 2, we display and compare representative PELDOR traces recorded with different experimental conditions. First, we compare the performance of the high- versus the low- Q probe head using a frequency separation of 60 MHz (Fig. 2b).

The detection was set at g_y of $\text{NH}_2\text{Y}_{731}\cdot$ (field position on the field-swept spectrum: 3352.8 mT, see Fig. 1) and the pumping at g_z , corresponding to $B = 3354.9$ mT. Each experiment was optimized for performance. The probe head with the higher quality factor combined with the availability of high microwave power (400 mW) provides better data quality (about twice larger S/N), although the cavity bandwidth is only about 20 MHz. The data indicate that the new commercial experimental setup allows larger frequency separation ($\Delta\nu = 60$ MHz) for PELDOR than reported in previous studies [10]. For this particular frequency separation, the π -pump pulses, measured 60 MHz from the dip center, are comparable in both low- and high- Q resonators (about 80–90 ns). Thus, the high- Q turns out to be the factor providing the best S/N ratio. Both traces exhibit the first maximum of the dipolar evolution function at 0.65 μs (Fig. 2b).

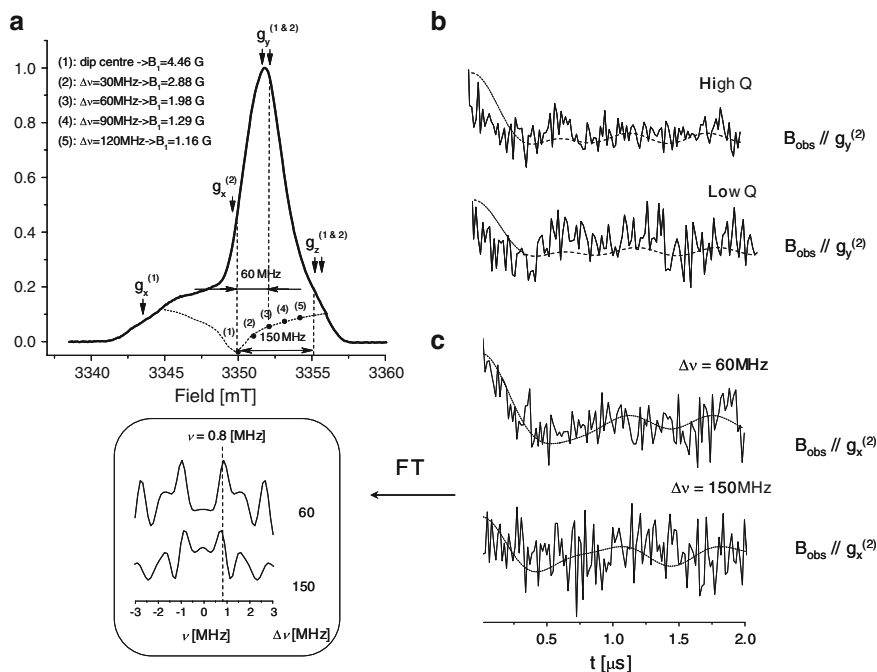


Fig. 2 **a** Measured B_1 microwave fields (determined by nutation experiments) for different $\Delta\nu$ values from the center of the cavity dip and relationship between possible frequency separation and the measured EPR spectral width. For $\Delta\nu = 150$ MHz, a full nutation period could not be recorded to measure B_1 due to the weakness of the signal, however, a spin echo was detectable. **b** Normalized dipolar evolution functions for the PELDOR experiments carried out with the high- and low- Q resonators; see the text for further details. **c** Comparison of time traces with detection at $g_x^{(2)}$ and different frequency separations. In **b** and **c** the *dotted* and *dashed* lines represent simulation with the radical structures discussed in the text. The modulation depth for the traces recorded with $\Delta\nu = 60$ MHz has been estimated up to 6% of the maximum echo signal; in the case of $\Delta\nu = 150$ MHz, the modulation depth is $<2\%$

To examine the effect of orientation selection, we first recorded a few traces with detection at the canonical points of the EPR spectrum and employing different frequency spacing, i.e., $\Delta\nu = 60$ and 150 MHz, respectively (Fig. 2c). We started with selective detection on g_x ($Y_{122}\cdot$) and subsequently shifted the detection versus g_y , while pumping at the higher-field side, respectively. We readily noted that no modulation could be observed in any traces until the detection reached g_x of $NH_2Y_{731}\cdot$, corresponding to the B_0 value of 3350.4 mT (see the field-swept spectrum, Fig. 2a), where finally some PELDOR modulation becomes visible. These traces are displayed in Fig. 2b and show a modulation frequency close to 1.6 MHz. On the other hand, the traces in Fig. 2c with $\Delta\nu = 60$ MHz and $\Delta\nu = 150$ MHz exhibit the first maximum of the dipolar evolution close to 1.3 μ s, corresponding to the modulation frequency $\nu_{\perp} = 0.8$ MHz. For the bottom trace of Fig. 2c, the modulation depth might be hardly distinguishable per visual inspection but a Fourier transformation (Fig. 2, inset, left) displays the mentioned frequency. Analogous results have been obtained with $\Delta\nu = 120$ MHz (data not shown), keeping the detection on g_x ($NH_2Y_{731}\cdot$), as described for the previous experiments.

In a second series of experiments we kept the frequency spacing fixed to $\Delta\nu = 60$ MHz and we recorded PELDOR traces as a function of the magnetic field position.

The data are shown in Fig. 3. Figure 3a shows the original time traces, whereas Fig. 3b shows Fourier transformation of the traces with non-zero modulation after background correction. For each trace, the detection field is indicated. From Fig. 3a, b some interesting features of the orientation selection become visible. Three regions can be distinguished: (1) a region between g_x ($Y_{122}\cdot$) and g_x ($NH_2Y_{731}\cdot$), in which, as mentioned above, no modulation is observed; (2) a region between g_x ($NH_2Y_{731}\cdot$) and g_y , in which a slow frequency component $\leq \nu_{\perp}$ (0.8 MHz) is observed; and (3) a region between g_y and g_z , in which the parallel component of the dipolar tensor, i.e., $\nu_{\parallel} = 1.6$ MHz, is visible.

The data reported in Figs. 2 and 3 show a quite complex pattern of orientation selection that can not be readily analyzed in terms of a biradical structure. A fitting procedure of the time traces in Fig. 3 using a home-written program reported in Ref. [12] was not feasible with arbitrary choices of starting Euler angles that define the orientations of the g -tensors to the dipolar axis. Indeed, the noise level is such that the fit routine (Matlab `fmincon`) would find only local minima close to the starting parameters. To overcome this problem and find reasonable starting simulation parameters, we examined the orientation of the two tyrosines, Y_{122} and Y_{731} , in the docking model of $\alpha 2$ and $\beta 2$ subunits in wild-type *E. coli* RNR [18]. The structure is depicted in Fig. 4. We point out that the mutation introduced at position 731 (one proton at C3 of the tyrosine ring is substituted with an amino group) in our system might alter the orientation of this residue in a way that is still unknown. Furthermore, in our experiment the enzyme is trapped in the active state with the essential residues Y_{122} and NH_2Y_{731} in the oxidized form, whereas the docking model is composed of the X-ray structures in the resting state. Thus, the structure illustrated in Fig. 4 might give some insight in the possible orientation of the radical pair, but is not identical to it.

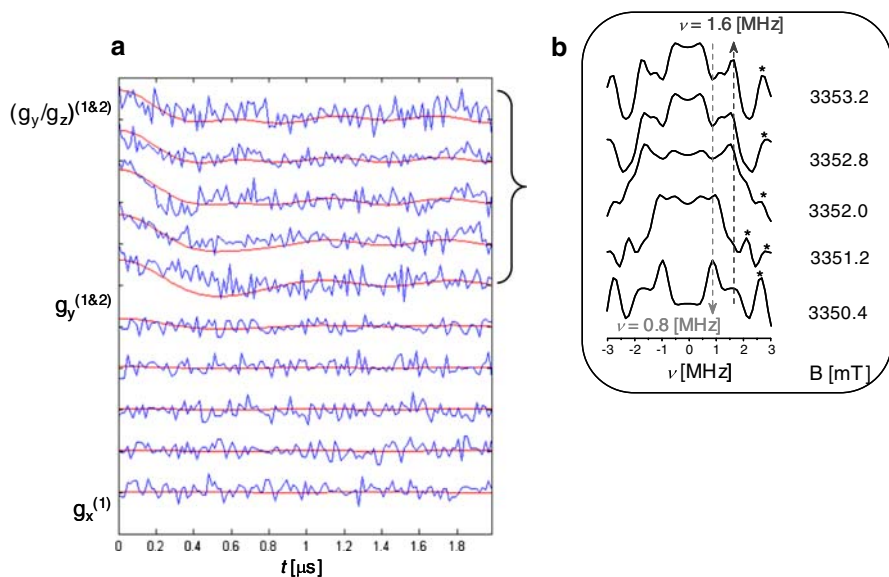


Fig. 3 **a** PELDOR traces registered as a function of the magnetic field. *Solid line* Simulation of each trace reported for the biradical structure described in the text. The concentration of the studied radical pair has been estimated as $<50 \mu\text{M}$. **b** Selected Fourier transformation after background correction for the field values specified on the *right*; a change in the ratio $\nu_{\perp}/\nu_{\parallel}$ is visible. *Asterisks* Artifacts produced by low S/N ratios

Figure 4 displays some interesting information that let us rationalize the most prominent features of the orientation selection in Figs. 2 and 3. First of all, none of the molecular axes between the two tyrosines are parallel. As the g -tensor axes in Y_{122} and also NH_2Y_{731} are collinear with the molecular axes, the two g -tensors are likely non-collinear as well. For this case, the probability of finding pairs of radicals by pumping and detecting at the canonical points of the EPR spectrum should be low, as indeed observed in the weak modulation of Figs. 2 and 3. Secondly, we examined the orientation of the two tyrosines with respect to the vector r , interconnecting the respective phenolic oxygen atoms. The direction of this vector should approximate the direction of the dipolar vector that in a point-dipole approximation connects the center of gravity of the spin densities. For Y_{122} , the vector r lies almost in the X/Z plane, forming an angle of 53° with the X axis. This angle accidentally almost matches the magic angle (54.74°), an angle between the external field and the dipolar vector, for which the dipolar frequency becomes zero. As a consequence, when the external field is parallel or close to X and thus g_x of Y_{122} , no modulation frequency might be observable. This hypothesis is in agreement with the experimental data in Figs. 2 and 3, which show no modulation for any selective detection in the g_x region of Y_{122} . For Y_{731} , r forms an angle of 73° with X and angles of 40° and 50° with the Y and Z axes, respectively. With the same argument provided for Y_{122} , as the latter angle is close to the magic angle, detection of NH_2Y_{731} at field positions close to g_z might lead to no detection of dipolar modulation.

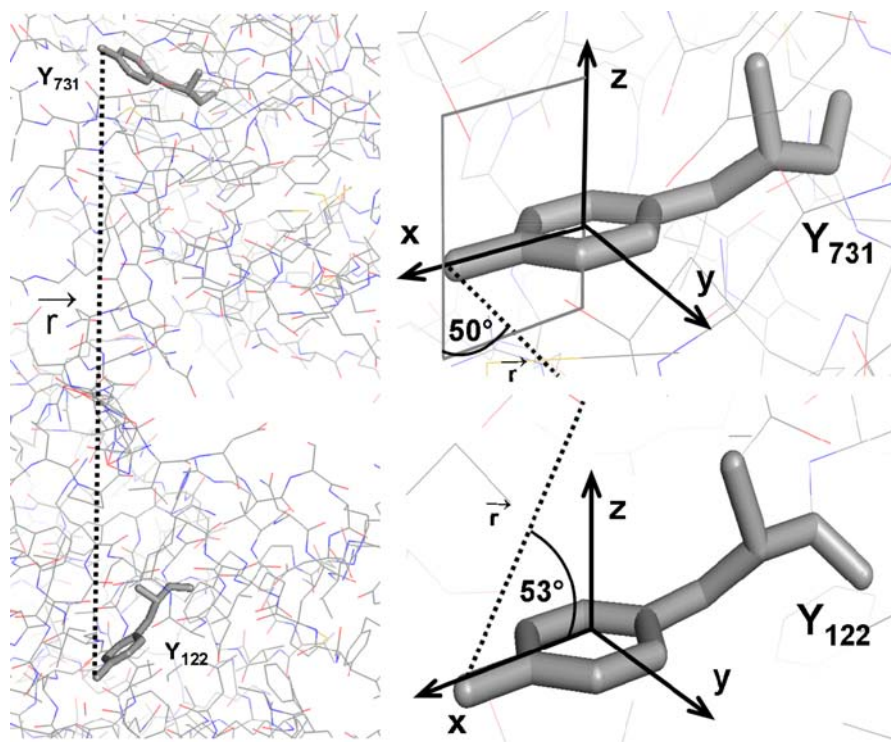


Fig. 4 *Left* Structure of the Y_{122} and Y_{731} pair as depicted from the docking model of the X-ray structures of $\alpha 2$ and $\beta 2$ [18]. It should be noted that the Y_{122} is one $\alpha\beta$ pair, while NH_2Y_{731} is in the adjacent $\alpha\beta$ pair. *Right* Orientation of the molecular axes with respect to the vector r , interconnecting the oxygens of the tyrosines. In the crystal structure both tyrosines are reduced. The orientations of r close to the magic-angle condition with the Z axis in Y_{731} and with the X axis in Y_{122} are illustrated, respectively

The orientation of the two tyrosines in Fig. 4 was used to test a simulation of the time traces in Fig. 3. All parameters have been independently established that determine the EPR line shape (hyperfine and g -tensors) [17], the pulse excitation bandwidth as well as the dipolar tensor [16]. Our simulation program thus requires only five input parameters, which define the Euler angles of two consecutive rotations. First we rotate the g -tensor of radical 2, here Y_{731} , into the dipolar tensor (rotation denoted as \mathbf{R}_d' in Ref. [12]); second, the dipolar tensor into the g -tensor of radical 1, rotation denoted \mathbf{R}_d . Our PELDOR experiments at X-band had shown that the width of the distance distribution is only about $\pm 1.2 \text{ \AA}$ and could be safely neglected in this analysis. The orientations displayed in Fig. 4 with the additional simplification that r is entirely parallel to the X/Z plane of Y_{122} and to the Y/Z plane of Y_{731} leads to the Euler angles (in radians) $\alpha = 0$, $\beta = 3.8$ and $\gamma = 0$ of \mathbf{R}_d , and further $\alpha = 4.71$, $\beta = 4.0$, $\gamma = 0$ of \mathbf{R}_d' . The simulation is displayed on top of the time traces of Figs. 2 and 3 and reproduces the different spectral regions of the plot quite well. However, optimization of the parameters through a fit procedure was unfortunately still not feasible at this stage due to the data quality.

4 Conclusions

We have reported the observation of 94 GHz orientation-selected PELDOR for a rigid radical pair with non-collinear g axes. For this case, PELDOR frequencies corresponding to both components of the dipolar tensor ν_{\perp} and ν_{\parallel} could be detected only in a very limited spectral region between the g_y and g_z values. Furthermore, the orientation of the dipolar vector with respect to the g -tensor played key role as well. If the angle of the dipolar tensor with one of the g axes approaches the magic angle (54.74°), no modulation effect is observed for the external field parallel to this particular g axis direction, as we observed here.

Although our experiments were performed with state-of-the-art commercial hardware for 94 GHz EPR, a quantitative analysis was still limited by the S/N ratio obtained. A simulation with orientation parameters from the docking model of the X-ray structures to reproduce the data satisfactorily, using a global fitting procedure to find an optimized biradical structure, was not feasible.

The S/N ratio is a critical issue when dealing with biological samples at low spin concentrations as in this example. One possibility to improve the S/N ratio consists in optimizing the efficiency of the pump pulse, which is currently limited by the high- Q of standard single-mode cylindrical cavities used in pulsed high-frequency EPR. Work in our group is in progress to construct a new bimodal resonator suited for PELDOR experiments.

Nevertheless, the current work provides one more example for the feasibility of high-frequency PELDOR and represents a further step toward the application of PELDOR spectroscopy in structural determination of biological systems.

Acknowledgments This work has been supported by the Deutsche Forschungsgemeinschaft priority programs SFB803 and IRTG 1422, and by the Max Planck Society and GM-29595 (J.S.).

Open Access This article is distributed under the terms of the Creative Commons Attribution Non-commercial License which permits any noncommercial use, distribution, and reproduction in any medium, provided the original author(s) and source are credited.

References

1. A.D. Milov, A.B. Ponomarev, Yu.D. Tsvetkov, *Chem. Phys. Lett.* **110**, 67–72 (1984)
2. M. Pannier, S. Veit, A. Godt, G. Jeschke, H.W. Spiess, *J. Magn. Reson.* **142**, 331–340 (2000)
3. G. Jeschke, *Macromol. Rapid Commun.* **23**, 227–246 (2002)
4. C. Elsässer, M. Brecht, R. Bittl, *J. Am. Chem. Soc.* **124**, 12606–12611 (2002)
5. O. Schiemann, T.F. Prisner, *Q. Rev. Biophys.* **40**, 1–53 (2007)
6. D. Goldfarb, Y. Lipkin, A. Potapov, Y. Gorodetsky, B. Epel, A.M. Raitsimiring, M. Radoul, I. Kaminker, *J. Magn. Reson.* **194**, 8–15 (2008)
7. W. Hofbauer, K.A. Earle, C.R. Dunnam, J.K. Moscicki, J.H. Freed, *Rev. Sci. Instrum.* **75**, 1194–1208 (2004)
8. G. Smith, P.A.S. Cruickshank, D.R. Bolton, D.A. Robertson, in *High Field Pulsed EPR Instrumentation*, ed. by B.C. Gilbert, M.J. Davies, D.M. Murphy. *Electron Paramagnetic Resonance*, vol 21 (RCS Publishing, Cambridge, 2008), pp. 216–233
9. V.P. Denysenkov, T.F. Prisner, J. Stubbe, M. Bennati, *Proc. Natl. Acad. Sci. USA* **103**, 13386–13390 (2006)

10. Y. Polyhach, A. Godt, C. Bauer, G. Jeschke, J. Magn. Reson. **185**, 118–129 (2007)
11. A. Savitsky, A.A. Dubinskii, M. Flores, W. Lubitz, K. Möbius, J. Phys. Chem. B **111**, 6245–6262 (2007)
12. V. Denysenkov, D. Biglino, W. Lubitz, T. Prisner, M. Bennati, Angew. Chem. Int. Ed. **47**, 1224 (2008)
13. V.P. Denysenkov, T.F. Prisner, J. Stubbe, M. Bennati, Appl. Magn. Reson. **29**, 375–389 (2005)
14. O. Schiemann, P. Cekan, D. Margraf, T. Prisner, S. Sigurdsson, Angew. Chem. Int. Ed. **48**, 3292–3295 (2009)
15. G. Sicoli, G. Mathis, S. Aci-Sèche, C. Saint-Pierre, Y. Boulard, D. Gasparutto, S. Gambarelli, Nucleic Acids Res. **37**, 3165–3176 (2009)
16. M. Seyedsayamdost, C. Chan, V. Mugnaini, J. Stubbe, M. Bennati, J. Am. Chem. Soc. **129**, 15748–15749 (2007)
17. M. Seyedsayamdost, T. Argirević, E. Minnihan, J. Stubbe, M. Bennati, J. Am. Chem. Soc. doi: [10.1021/ja903879w](https://doi.org/10.1021/ja903879w)
18. U. Uhlin, H. Eklund, Nature **370**, 533–539 (1994)